

# FRACTIONAL ORDER PID DESIGN FOR ROBOTIC NON-LINEAR MOTION CONTROL

Yuequan Wan, Haiyan Henry Zhang, Richard Mark French, Purdue University

## Abstract

The modeling of multilink robots produces typical nonlinear systems with uncertain disturbances and high-order matrices. The authors present a method of applying a fractional-order PID controller to such a nonlinear system and show the advantages of this fractional controller. In this study, the dynamic model of the system served as the foundation to derive the control law and objective function for the optimization design of the subjected fractional-order control system. The frequency domain closed-loop transaction function of this fractional system was developed and is discussed here along with controllability, observability and robust satiability. The authors demonstrated the use of algorithms to design and optimize the fractional-order PID to the nonlinear motion control system. By conducting a series of numerical computations, the authors showed that the fractional-order PID controller could enlarge the stable region of a multilink robot system and, therefore, deliver superior control performance in terms of trajectory tracking. The results and procedures introduced here could be practically generalized to other similar systems.

## Introduction

Multilink robots are widely used in the manufacturing industry, and the motion control issues of these robot systems have become popular research topics for decades since the first appearance of the robots in industry. Generally speaking, multilink robot systems typically are nonlinear and always involve disturbances. The fine control of industrial robots usually requires complex control systems, careful calibrations and optimizations. In practice, most of these multilink robots are controlled by PID controllers which have the merits or effectiveness, simplicity and feasibility. Although ordinary PID controllers can achieve satisfactory results in most common manufacturing missions, they still lack enough precision in the field and often require precise instrument control.

The ordinary PID controller is designed to provide the restoring, corrective and counteractive forces to the controlled system. In typical situations, the ordinary PID controller can always effectively achieve the control objectives without obvious drawbacks. However, in modern industry,

the demand for precise control is driving people to search for improvements. Fractional-order PID (FoPID) introduced here is a natural extension to ordinary PID controllers based on the fractional calculus theory. Since in fractional calculus the orders of integral and derivative are not limited to integer orders anymore, a new type of PID controller can be introduced by replacing the ordinary order integrators and differentiators with fractional-order ones. The main advantages of the FoPID controllers include an enlarged stable region, relatively feasible structure and raised control precision.

As mentioned above, fractional calculus takes the order of integrals and derivatives as any real number. It has a history nearly as long as ordinary calculus, which considers only integer orders [1]. Recently, successful applications of this technology have been found in many fields, such as viscoelasticity [2], [3], control theory [4], [5] and electro-analytical chemistry [6], [7]. In control theory, the general conclusion about a fractional control system is that it could enlarge the stable region [8] and yield a performance at least as good as its integer counterpart. Another important advantage is that fractional integrals or derivatives are hereditary functional while the ordinary ones are point functional. It is known that the hereditary function has a long memory characteristic [9], which means that at any time it would process a total memory of past states. This unique characteristic serves as one of the important reasons for its better performance. For FoPID controllers, many scholars have made tremendous contributions in recent years [10], especially in the tuning rules [11], [12], approximation [13] and stability conditions [14]. These previous studies drove the foundation for the work done in this study.

In this study, then, the authors applied FoPID controllers to a nonlinear multilink robot system and take uncertain disturbances into consideration. Furthermore, the fractional orders of the integrators and differentiators used here are considered as design variables rather than pre-defined parameters. The authors studied the stability conditions and optimization design method for the overall comprehensive performance of the FoPID controllers on the basis of the mathematical model of an Adept 550 robot [15]. Adept 550 is widely used in the industry. It has four axes with three rotational joints and one translational joint. Its beauty lies in its small motion envelope, high speeds and payloads. These

features make the Adept 550 robot a feasible tool for fast and precise operations in production lines, such as subassembly and assembly, packaging and even driving screws. The authors' complete study of FoPID controllers using the Adept 550 robot shows that the fractional controller could achieve high precise control and bring feasible approaches to optimize the design of the FoPID in other applications.

## Dynamic Model of an Adept 550 Robot

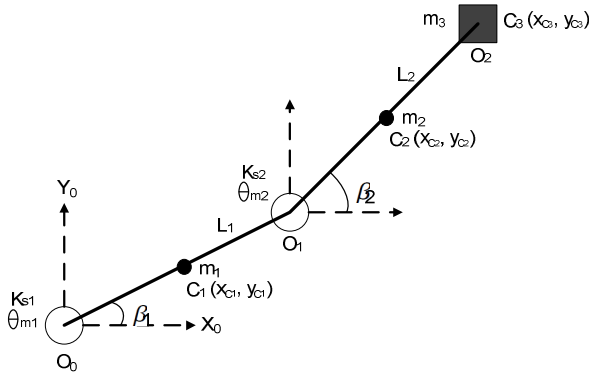


Figure 1. Simplified Structure of Adept 550 Robot

Table 1. D-H Parameters

Link	$L_i$	$i$	$d_i$	$i$
Inner	L1	0	0	1
Outer	L2	0	0	2

$$A_i = R_{z,\theta_i} T_{z,d_i} T_{x,L_i} R_{x,\alpha_i} = \begin{bmatrix} \cos\theta_i & -\sin\theta_i \cos\alpha_i & \sin\theta_i \sin\alpha_i & L_i \cos\theta_i \\ \sin\theta_i & \cos\theta_i \cos\alpha_i & -\cos\theta_i \sin\alpha_i & L_i \sin\theta_i \\ 0 & \sin\alpha_i & \cos\alpha_i & d_i \\ 0 & 0 & 0 & 1 \end{bmatrix} \quad (1)$$

The simplified structure of an Adept 550 robot is shown in Figure 1. When applying Denavit-Hartenberg (D-H) coordinates to Adept 550, one can see the special case of parallel  $z$  axes. Its inner and outer links are assumed to be rigid bodies, whose motion determines the trajectory of this robot. Its trajectory is not affected by the gripper angle adjustment during the rotation of the wrist. Without loss of generality, the wrist's rotary angle is assumed to be zero, thus the study could focus on the performance of trajectory tracking. Assuming the notations shown in Figure 1, and using the D-H parameters of the inner ( $i=1$ ) and outer ( $i=2$ ) links from Table 1, the following matrix describes the coordinate transformation of rotation and translation:

The subsequent transformation matrix from the base to the gripper can be derived as:

$$T_0^2 = A_1 A_2 = \begin{bmatrix} \cos(\theta_1 + \theta_2) & -\sin(\theta_1 + \theta_2) & 0 & L_1 \cos\theta_1 + L_2 \cos(\theta_1 + \theta_2) \\ \sin(\theta_1 + \theta_2) & \cos(\theta_1 + \theta_2) & 0 & L_1 \sin\theta_1 + L_2 \sin(\theta_1 + \theta_2) \\ 0 & 0 & 1 & 0 \\ 0 & 0 & 0 & 1 \end{bmatrix} \quad (2)$$

The gripper's horizontal position ( $P_x, P_y$ ) can be expressed as

$$\begin{aligned} P_x &= L_1 \cos \beta_1 + L_2 \cos \beta_2 \\ P_y &= L_1 \sin \beta_1 + L_2 \sin \beta_2 \end{aligned} \quad (3)$$

where  $\beta_i$  ( $i = 1, 2$ ) is the angular position of the motors, and  $\theta_i$  ( $i = 1, 2$ ) is the angle about previous  $z$  from old  $x$  to new  $x$ . The relationships of them are described as  $\beta_1 = \theta_1$ ,  $\beta_2 = \theta_1 + \theta_2$ . Thus, we have the motor's angular positions ( $\beta_1, \beta_2$ ), forward velocity  $v$  and backward velocity ( $\dot{\beta}_1, \dot{\beta}_2$ ), and backward acceleration ( $\ddot{\beta}_1, \ddot{\beta}_2$ ) [15]:

$$\begin{aligned} \beta_1 &= 2 \tan^{-1} \left( \frac{P_y \pm \sqrt{P_x^2 + P_y^2 - R_1}}{P_x + R_1} \right) \\ \beta_2 &= 2 \tan^{-1} \left( \frac{P_y \pm \sqrt{P_x^2 + P_y^2 - R_2}}{P_x + R_2} \right) \end{aligned} \quad (4)$$

where

$$\begin{aligned} R_1 &= \frac{P_x^2 + P_y^2 + L_1^2 - L_2^2}{2L_1} \\ R_2 &= \frac{P_x^2 + P_y^2 + L_2^2 - L_1^2}{2L_2} \end{aligned} \quad (5)$$

$$v = \begin{pmatrix} \dot{P}_x \\ \dot{P}_y \end{pmatrix} = J_a \begin{pmatrix} \dot{\beta}_1 \\ \dot{\beta}_2 \end{pmatrix} \quad (6)$$

and where  $J_a$  is a Jacobian matrix

$$J_a = \begin{bmatrix} -L_1 \sin \beta_1 & -L_2 \sin \beta_2 \\ L_1 \cos \beta_1 & L_2 \cos \beta_2 \end{bmatrix} \quad (7)$$

$$\begin{pmatrix} \dot{\beta}_1 \\ \dot{\beta}_2 \end{pmatrix} = J^{-1} \begin{pmatrix} \dot{P}_x \\ \dot{P}_y \end{pmatrix} \quad (8)$$

$$\begin{pmatrix} \ddot{P}_x \\ \ddot{P}_y \end{pmatrix} = J_a \begin{pmatrix} \ddot{\beta}_1 \\ \ddot{\beta}_2 \end{pmatrix} + J_v \begin{pmatrix} \dot{\beta}_1 \\ \dot{\beta}_2 \end{pmatrix} \quad (9)$$

and where

$$J_v = \begin{bmatrix} -L_1 \cos \beta_1 & -L_2 \cos \beta_2 \\ -L_1 \sin \beta_1 & -L_2 \sin \beta_2 \end{bmatrix} \quad (10)$$

$$\begin{pmatrix} \ddot{\beta}_1 \\ \ddot{\beta}_2 \end{pmatrix} = J_a^{-1} \begin{pmatrix} \ddot{P}_x \\ \ddot{P}_y \end{pmatrix} - J_a^{-1} J_v \begin{pmatrix} \dot{\beta}_1^2 \\ \dot{\beta}_2^2 \end{pmatrix} \quad (11)$$

Applying the Lagrange method, the dynamics of the Adept 550 robot can be described [15] as:

$$D(\beta)\ddot{\beta} + H(\beta, \dot{\beta})\dot{\beta} + G(\beta) = \tau + \tau_{damping} \quad (12)$$

where

$$D(\beta) = \begin{bmatrix} \left(\frac{7}{12}m_1 + m_2 + m_3\right)L_1^2 & \left(\frac{1}{2}m_2 + m_3\right)L_1L_2 \cos(\beta_2 - \beta_1) \\ \left(\frac{1}{2}m_2 + m_3\right)L_1L_2 \cos(\beta_2 - \beta_1) & \left(\frac{7}{12}m_2 + m_3\right)L_2^2 \end{bmatrix} \quad (13a)$$

$$H(\beta, \dot{\beta}) = \begin{bmatrix} 0 & -\left(\frac{1}{2}m_2 + m_3\right)L_1L_2 \sin(\beta_2 - \beta_1)\dot{\beta}_2 \\ \left(\frac{1}{2}m_2 + m_3\right)L_1L_2 \sin(\beta_2 - \beta_1)\dot{\beta}_1 & 0 \end{bmatrix} \quad (13b)$$

$$G(\beta) = \begin{pmatrix} \left(\frac{1}{2}m_1 + m_2 + m_3\right)gL_1 \cos \beta_1 - k_{s1}(r\theta_{m1} - \beta_1) \\ \left(\frac{1}{2}m_2 + m_3\right)gL_2 \cos \beta_2 - k_{s2}(r\theta_{m2} - \beta_2) \end{pmatrix} \quad (13c)$$

$$\tau = \begin{pmatrix} \tau_1 \\ \tau_2 \end{pmatrix} \quad (13d)$$

$$\tau_{damping} = \begin{pmatrix} \tau_{damping1} \\ \tau_{damping2} \end{pmatrix} = \begin{bmatrix} -C_1 & 0 \\ 0 & -C_2 \end{bmatrix} \begin{pmatrix} \dot{\beta}_1 \\ \dot{\beta}_2 \end{pmatrix} = C \begin{pmatrix} \dot{\beta}_1 \\ \dot{\beta}_2 \end{pmatrix} \quad (13e)$$

The damping coefficients are included in matrix  $C$ .

## Model of Fractional-order PID Controllers

Based on Equation (12), it can be assumed that the motors driving the inner and outer links are of the same type. Dynamics of the two link for  $k = 1, 2$  is described as:

$$\sum_{j=1}^n d_{jk}(\beta)\ddot{\beta}_j + \sum_{i,j=1}^n h_{ijk}(\beta)\dot{\beta}_i\dot{\beta}_j + g_k(\beta) = \tau_k - C_k\dot{\beta}_k, \quad (14)$$

$$J_{m,k}\ddot{\theta}_{mk} + \left(B_{m,k} + K_{b,k} \frac{K_{m,k}}{R_k}\right)\dot{\theta}_{mk} = \frac{K_{m,k}}{R_k}V_k - \tau_{m,k}$$

Since  $\beta_k = r\theta_{m,k}$ ,  $\tau_{m,k} = r\tau_k$ , where  $r$  is the gear ratio, the two dynamic equations of robot link and its driving motor expressed in Equation (14) can be combined into a single equation:

$$J_{eff,k}\ddot{\theta}_{mk} + B_{eff,k}\dot{\theta}_{mk} = KV_k - C_k\theta_{mk} - rd_k \quad (15)$$

Now, for a fractional-order PID controller,  $PI^\lambda D^\mu$ , one gets the five design parameters summarized in Table 2.

**Table 2. Design Parameters for the Controller**

$K_p$	Coefficient for the proportional term
$K_D$	Coefficient for the derivative term
$K_I$	Coefficient for the integral term
$\mu$	Fractional order for the derivative term
$\lambda$	Fractional order for the integral term

The closed-loop control diagram is shown in Figure 2, while Equation (16) describes the transfer function of this closed-loop system. The fractional derivative used in this study is defined as Caputo's fractional derivative [16].

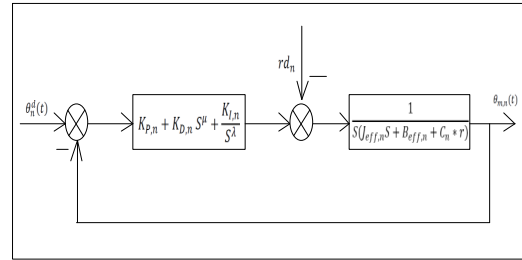


**Figure 2. Closed-Loop Diagram of Fractional-Order,  $PI^\lambda D^\mu$  Controlled Robot Arm**

$$\theta_{m,n} = \frac{(K_p \theta_n^d - rd_n)S^\lambda + K_{I,n}\theta_n^d}{J_{eff,n}S^{\lambda+2} + (B_{eff,n} + C_n r)S^{\lambda+1} + K_{p,n}S^\lambda + K_{I,n}} \quad (16)$$

In this study, the FoPID controllers of the two arms had the same fractional order,  $\lambda$  and  $\mu$ , and different coefficients. Besides, both the fractional order of the integrator and the differentiator are bounded in the range of (0, 1) in this study. In Equation (16), the non-linear terms,  $d_n$ , are non-linear disturbances given as:

$$\begin{aligned} d_1 &= \left(\frac{1}{2}m_2 + m_3\right)\{L_1L_2 \cos(\beta_2 - \beta_1)\ddot{\beta}_2 \\ &\quad - L_1L_2 \sin(\beta_2 - \beta_1)\dot{\beta}_2^2\} + \left(\frac{1}{2}m_1 + m_2 + m_3\right)gL_1 \cos \beta_1 \\ d_2 &= \left(\frac{1}{2}m_2 + m_3\right)\{L_1L_2 \cos(\beta_2 - \beta_1)\ddot{\beta}_1 \\ &\quad - L_1L_2 \sin(\beta_2 - \beta_1)\dot{\beta}_1^2 + gL_2 \cos \beta_2 \end{aligned} \quad (17)$$

Apply Caputo's fractional-order derivative to Equation (17), and given  $\beta_K = r\theta_{m,K}$ , the time domain system function could be represented by the following matrix.

$$\begin{aligned} & \begin{bmatrix} J_{eff,1} & r^2 T_1 \\ r^2 T_1 & J_{eff,2} \end{bmatrix} \begin{bmatrix} {}_0 D_t^{\lambda+2} \beta_1 \\ {}_0 D_t^{\lambda+2} \beta_2 \end{bmatrix} + \begin{bmatrix} B_{eff,1} + c_1 r & r^2 T_2 \beta_2^{2-\lambda} \\ r^2 T_2 \beta_1^{2-\lambda} & B_{eff,2} + c_2 r \end{bmatrix} \begin{bmatrix} {}_0 D_t^{\lambda+2} \beta_1 \\ {}_0 D_t^{\lambda+2} \beta_2 \end{bmatrix} + \\ & \begin{bmatrix} K_{p1} + r^2(-T_3 \beta_2 + T_4 \beta_2^2 + T_5) & r^2(T_3 \beta_2 - T_4 \beta_2^2) \\ r^2(-T_3 \beta_1 + T_4 \beta_1^2) & K_{p2} + r^2(T_3 \beta_1 - T_4 \beta_1^2 + T_6) \end{bmatrix} \begin{bmatrix} {}_0 D_t^{\lambda} \beta_1 \\ {}_0 D_t^{\lambda} \beta_2 \end{bmatrix} \\ & + \begin{bmatrix} K_{D1} & 0 \\ 0 & K_{D2} \end{bmatrix} \begin{bmatrix} {}_0 D_t^{\lambda+\mu} \beta_1 \\ {}_0 D_t^{\lambda+\mu} \beta_2 \end{bmatrix} + \begin{bmatrix} K_{I1} & 0 \\ 0 & K_{I2} \end{bmatrix} \begin{bmatrix} \beta_1 \\ \beta_2 \end{bmatrix} = \\ & = \begin{bmatrix} K_{p1} & 0 \\ 0 & K_{p2} \end{bmatrix} \begin{bmatrix} {}_0 D_t^{\lambda} \beta_1^d \\ {}_0 D_t^{\lambda} \beta_2^d \end{bmatrix} + \begin{bmatrix} K_{D1} & 0 \\ 0 & K_{D2} \end{bmatrix} \begin{bmatrix} {}_0 D_t^{\lambda+\mu} \beta_1^d \\ {}_0 D_t^{\lambda+\mu} \beta_2^d \end{bmatrix} + \begin{bmatrix} K_{I1} & 0 \\ 0 & K_{I2} \end{bmatrix} \begin{bmatrix} {}_0 D_t^{\lambda} \beta_1^d \\ {}_0 D_t^{\lambda} \beta_2^d \end{bmatrix} \end{aligned} \quad (18)$$

where

$$T_1 = \left( \frac{1}{2} m_2 + m_3 \right) L_1 L_2 \cos(\beta_2 - \beta_1) \quad (19a)$$

$$T_2 = - \left( \frac{1}{2} m_2 + m_3 \right) L_1 L_2 \sin(\beta_2 - \beta_1) \frac{\Gamma(3)}{\Gamma(3-\lambda)} \quad (19b)$$

$$T_3 = \left( \frac{1}{2} m_2 + m_3 \right) L_1 L_2 \cos(\beta_2 - \beta_1 + \lambda \frac{\pi}{2}) \quad (19c)$$

$$T_4 = \left( \frac{1}{2} m_2 + m_3 \right) L_1 L_2 \sin(\beta_2 - \beta_1 + \lambda \frac{\pi}{2}) \quad (19d)$$

$$T_5 = \left( \frac{1}{2} m_1 + m_2 + m_3 \right) g L_1 \cos(\beta_1 + \lambda \frac{\pi}{2}) \quad (19e)$$

$$T_6 = \left( \frac{1}{2} m_2 + m_3 \right) g L_2 \cos(\beta_2 + \lambda \frac{\pi}{2}) \quad (19f)$$

In Equation (18), the differential order of  $\beta_1$   $\beta_2$  is  $\lambda + 2$ ,  $\lambda + 1$ ,  $\lambda + \mu$  and 0. Since these orders are not equally spaced, it is not easy to directly re-write Equation (18) in a linear matrix formation. Inspired by the work of Galkowski et al. [17], it was assumed that  $\lambda$  and  $\mu$  are rational numbers, which could be expressed by  $a/b$  and  $c/d$  and in their relatively prime formats, respectively. By noting that  $\beta = [\beta_1 ; \beta_2]$ , Equation (18) could be written as:

$$M_{10} D_t^{\frac{ac+2bd}{bd}} \beta + M_{20} D_t^{\frac{ac+bd}{bd}} \beta + M_{30} D_t^{\frac{ac+bc}{bd}} \beta + M_{40} D_t^{\frac{ad}{bd}} \beta + M_{50} D_t^0 \beta - U = 0 \quad (20)$$

In Equation (20),  $M_i$  and  $U$  make up a coefficient matrix with their corresponding terms in Equation (18). One more thing to mention here is that not all of these coefficients are constant, given the uncertain disturbance. Equation (20) actually will be shown later to be a time variant system. By inserting zero matrixes, it is equivalent to rewriting Equation (20) as shown follows:

$$\begin{aligned} & M_{10} D_t^{\frac{ac+2bd}{bd}} \beta + N_{10} D_t^{\frac{ac+2bd-1}{bd}} \beta + N_{20} D_t^{\frac{ac+2bd-2}{bd}} \beta + \dots + M_{20} D_t^{\frac{ac+bd}{bd}} \beta + \\ & + N_{i0} D_t^{\frac{ac+bd-1}{bd}} \beta + \dots + M_{30} D_t^{\frac{ac+bc}{bd}} \beta + \dots + N_{j0} D_t^{\frac{ad+1}{bd}} \beta + \\ & + M_{40} D_t^{\frac{ad}{bd}} \beta + \dots + N_{k0} D_t^{\frac{a+1}{bd}} \beta + M_{50} D_t^0 \beta - U = 0 \end{aligned} \quad (21)$$

where  $N_1 = N_2 = \dots = N_i = \dots = N_j = N_k = 0$ .

Based on Equation (21) one has an equally spaced fractional-order system on every term and, therefore, the state space could be defined as:

$$x = \left[ {}_0 D_t^0 \beta \quad {}_0 D_t^{\frac{1}{bd}} \beta \quad \dots \quad {}_0 D_t^{\frac{ad-1}{bd}} \beta \quad {}_0 D_t^{\frac{ad}{bd}} \beta \quad \dots \quad {}_0 D_t^{\frac{ad+2bd-1}{bd}} \beta \right]^T \quad (22)$$

The entire system, then, is:

$${}_0 D_t^{\frac{1}{bd}} X = AX + BU \quad (23)$$

where

$$A = \begin{bmatrix} 0_{[2ad+4bd-2,2]} & \vdots & I_{[2ad+4bd-2,2ad+4bd-2]} \\ \dots & \dots & \dots \\ -M_1^{-1} M_5 & 0 \dots -M_1^{-1} M_4 & 0 \dots -M_1^{-1} M_3 & 0 \dots -M_1^{-1} M_2 & 0 \dots \end{bmatrix} \quad (24a)$$

$$B = \begin{bmatrix} 0_{[2ad+4bd-2,2]} \\ \dots \\ 1 & 0 \\ 0 & 2 \end{bmatrix} \quad (24b)$$

In Equations (24.a) and (24.b),  $0_{[2ad+4bd-2,2]}$  is a zero matrix whose dimension is  $[2ad + 4bd - 2, 2]$  and  $I_{[2ad+4bd-2,2ad+4bd-2]}$  is the identity matrix having the dimension of  $[2ad + 4bd - 2, 2ad + 4bd - 2]$ . Equation (23) is the state space representation of our system function. The system matrix  $A$  has the dimension of  $[2ad + 4bd, 2ad + 4bd]$  and  $B$  has the dimension of  $[2ad + 4bd, 2]$ . The stability study and the design of the fractional-order PID controller will focus on the matrix  $A$ . Although  $A$  could have a very high dimension with a different fractional order, the fact that matrix  $A$  is a sparse matrix makes the task easier in most cases.

## Controllable, Observable and Robust Stability of the System

Since matrix  $A$  is in the controllable canonical form, and consequently one state could be transferred to another, the system is controllable and observable. The design focuses on the robust stability of this system. For a fractional-order system, the system would be guaranteed stable if all of the system matrix's eigenvalues satisfy the following criteria [18].

$$|\arg(\lambda)| > \beta \frac{\pi}{2} \quad (25)$$

Therefore, in this study, the ratio of the stable region of the FoPID to the integer PID is  $2-1/bd$ . One could raise  $b$  and  $d$  to get a larger stable region; however, raising them would cause a larger dimension of matrix  $A$  and involve more eigenvalues since the total number of eigenvalues is  $2ad+4bd$ . More eigenvalues would make it harder to guarantee that all of them are settled in the stable region.

Moreover, since  $A$  is a bounded sparse matrix with interval uncertainties, there should be an infinite number of eigenvalues to check to satisfy the stable region if one directly uses the method of Equation (25). In this case, boundaries of each eigenvalue [18], [19] should be checked and the stability of the system—based on the behaviors of all eigenvalue boundaries [20]—continually analyzed. Therefore, the boundaries of this system, matrix  $A$ , need to be checked. Based on Equations (18) and (19), the following inequality holds:

$$J_{eff,1}J_{eff,2} > r^2 J_m [L_1^2 (\frac{1}{2}m_1 + m_2 + m_3) + L_2^2 (\frac{1}{2}m_2 + m_3)] + r^4 (\frac{1}{2}m_2 + m_3)^2 L_1^2 L_2^2 \quad (26)$$

Thus, the determinant of matrix,  $M_1$ , satisfies the condition

$$J_{eff,1}J_{eff,2} - r^4 T_1^2 \neq 0 \quad (27)$$

The fact that the condition in Equation (27) always holds, implies that matrix  $M_1$  is always nonsingular and, consequently, matrix  $A$  will never be singular if  $K_{I1} \neq 0$ ,  $K_{I2} \neq 0$ . In this design, the authors kept this condition. Thus, one gets

$$\frac{1}{\det(M_1)} \in \left[ \frac{1}{J_{eff,1}J_{eff,2}}, \frac{1}{J_{eff,1}J_{eff,2} - r^4 (0.5m_2 + m_3)^2 L_1^2 L_2^2} \right] \quad (28)$$

In this robot control study,  $\beta$  and  $\hat{\beta}$  are also bounded because of reality. Therefore, one should also find that matrix  $A$  is bounded. Plugging in the parameters used in this study, one gets the following boundary functions for each variant term in  $A$  through numerical computation, where the boundaries are functions of the design parameters  $(K_{I1}, K_{I2}, K_{P1}, K_{P2}, K_{D1}, K_{D2}, \lambda, \mu)$ .

$$\begin{aligned} \overline{-M_1^{-1}M_5} &= \begin{bmatrix} -57.2273K_{I1} & 94.6367K_{I2} \\ 94.6367K_{I1} & -229.4504K_{I2} \end{bmatrix} \\ \underline{-M_1^{-1}M_5} &= \begin{bmatrix} -83.7362K_{I1} & -64.9431K_{I2} \\ -64.9431K_{I1} & -335.73674K_{I2} \end{bmatrix} \end{aligned} \quad (29a)$$

$$\begin{aligned} \overline{-M_1^{-1}M_4} &= \begin{bmatrix} 48.1076-71.7260K_{P1} & 27.5032+93.6562K_{P2} \\ 87.6325+71.3310K_{P1} & 98.6555-2623100K_{P2} \end{bmatrix} \\ \underline{-M_1^{-1}M_4} &= \begin{bmatrix} -44.5903-80.7186K_{P1} & -31.5653-64.9431K_{P2} \\ -96.3535-46.8943K_{P1} & -91.9135-308934K_{P2} \end{bmatrix} \end{aligned} \quad (29b)$$

$$\begin{aligned} \overline{-M_1^{-1}M_3} &= \begin{bmatrix} -57.2273K_{D1} & 94.6367K_{D2} \\ 94.6367K_{D1} & -229.4504K_{D2} \end{bmatrix} \\ \underline{-M_1^{-1}M_3} &= \begin{bmatrix} -83.7362K_{D1} & -64.9431K_{D2} \\ -64.9431K_{D1} & -335.73674K_{D2} \end{bmatrix} \end{aligned} \quad (29c)$$

$$\begin{aligned} \overline{-M_1^{-1}M_2} &= \begin{bmatrix} -5.7227+0.0711\hat{\beta}_{1,MAX}^{2-\lambda} & 9.4637 \\ 9.4637+0.2069\hat{\beta}_{1,MAX}^{2-\lambda} & -22.945+0.0609\hat{\beta}_{2,MAX}^{2-\lambda} \end{bmatrix} \\ \underline{-M_1^{-1}M_2} &= \begin{bmatrix} -8.3736 & -6.4943-0.4241\hat{\beta}_{2,MAX}^{2-\lambda} \\ -6.4943-1.7004\hat{\beta}_{1,MAX}^{2-\lambda} & -33.5737 \end{bmatrix} \end{aligned} \quad (29d)$$

Now, the robust stability of this FoPID controlled system at different design parameters could be studied  $(K_{I1}, K_{I2}, K_{P1}, K_{P2}, K_{D1}, K_{D2}, \lambda, \mu)$ . And this feature actually provides a criterion for optimizing the design of the controllers. Next, though, the authors would like to show how the design parameters, which are the coefficients and the fractional order of the two FoPID controllers, affect robust stability. Figure 3 shows this effect. Taking the upper left frame in Figure 3 as an example, the rectangles drawn by blue solid lines show the boundaries of each eigenvalue. Since there are uncertainties involved in this system, the eigenvalues are actually located in a range rather than single spots. And rectangles provide sufficient boundaries for these eigenvalues [19]. To ensure that the system is robustly stable, the eigenvalues' boundaries are not allowed to cross the stable boundary, which essentially is represented by the angle  $\pm 2\pi/bd$  in this study. For a better demonstration, the non-violated stable boundaries are plotted by cyan solid lines and those violated stable boundaries by red solid lines.

Figure 3 clearly shows that changing the combination of the design variables can change the overall stability of the system. During the design of the entire set of parameters, there could be unlimited permutations for the choices of design variable set  $(K_{I1}, K_{I2}, K_{P1}, K_{P2}, K_{D1}, K_{D2}, \lambda, \mu)$ . The authors would like to apply some optimization algorithm to achieve the comprehensive optimized design. Since the task of optimization design involves the permutation of each parameter, the genetic algorithm is a natural choice for this mission.

## Optimization Design

For this design, the system contains uncertainties and one could only obtain the ranges for each eigenvalue. As shown in Figure 3, the ranges are the rectangles bounded by the four corner eigenvalues. Drawing down these corner eigenvalues in a complex plane and noting their arguments by  $\angle\beta_{ij}, i=1,2,\dots,n; j=1,2,3,4$ , one could then measure the difference between these arguments and the stable boundary. In this way, and combined with the fact that all eigenvalues are symmetrical to the real axis in the complex plan, a natural optimization objective is to minimize the difference of stable arguments,  $2\pi/bd$ , to the absolute value of each  $\angle\beta_{ij}$

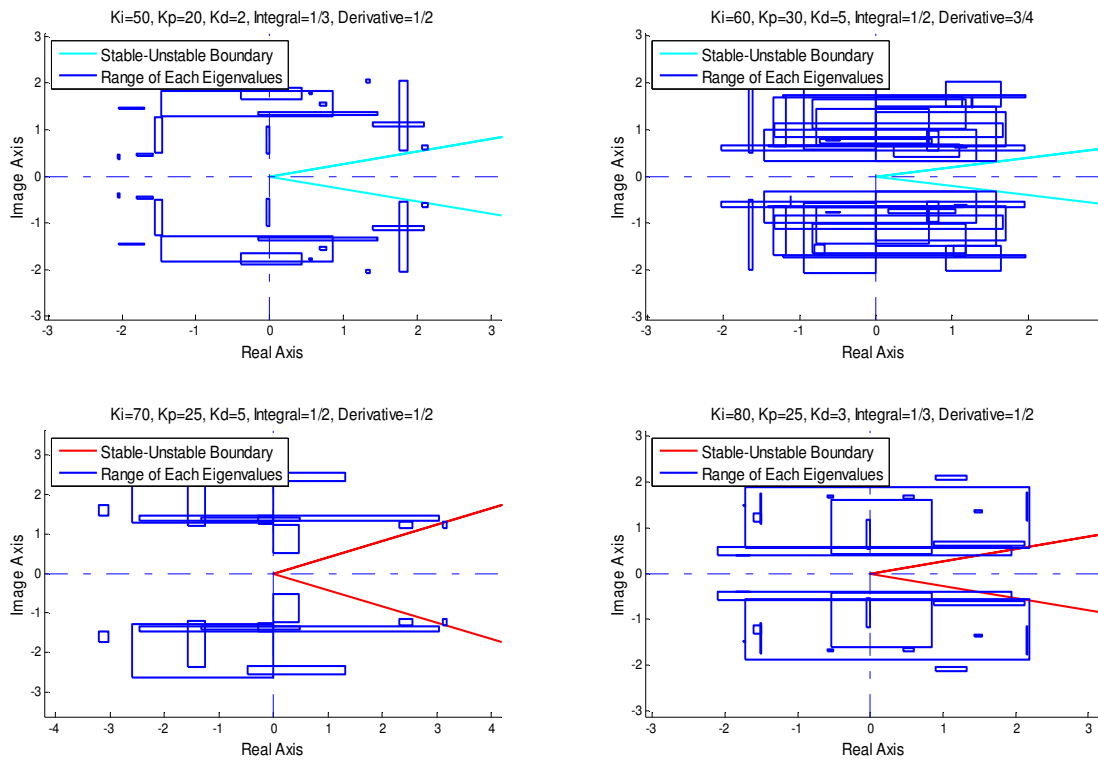


**Figure 3. Effect of Changing Design Variables on Overall Stability**

Therefore, the optimization function used in this research can be expressed as follows:

$$\begin{aligned}
 & \text{OptimalDesign}(K_{I1}, K_{I2}, K_{P1}, K_{P2}, K_{D1}, K_{D2}, \lambda, \mu) \\
 & = \arg \min \sum_{i=1}^n \sum_{j=1}^4 \psi_{ij} \left( \frac{2\pi}{bd} - |\angle \beta_{ij}| \right) \quad (30)
 \end{aligned}$$

In Equation (30),  $\psi_{ij}$  serves as the coefficient of penalization. There could be many methods used to assign the values of  $\psi_{ij}$ , and one could separate the complex plane into different segments according to various criteria. Here, the authors looked at the two-zone and three-zone stepwise penalization methods. Table 3 summarizes these two methods.

**Table 3. Value of Penalization Coefficient**

Two-Zone Method		Three-Zone Method	
$ \angle \beta_{ij} $	$\psi_{ij}$	$ \angle \beta_{ij} $	$\psi_{ij}$
$\in [0, 2\pi/bd]$	$1e+5$	$\in [0, 2\pi/bd]$	$1e+10$
$\in (2\pi/bd, \pi]$	1	$\in (2\pi/bd, 0.5\pi + 2\pi/bd]$	$1e+3$
N/A	N/A	$\in (0.5\pi + 2\pi/bd, \pi]$	1

Before exploring the trajectory tracking performance, the trajectory planning method used in this study will be introduced. First, let the robot arm move in both the x- and y-directions. Next, set the original point at 500mm by 320mm and allow 1 second for the robot arm to move to position 200mm by 600mm. Figure 4 demonstrates the trajectory plan. Table 4 summarizes the optimization results.

**Table 4. Optimization Results of Design Parameters**

Two-Zone Method		Three-Zone Method	
$K_{P1}$	146.93	$K_{P1}$	93.87
$K_{P2}$	14.27	$K_{P2}$	80.60
$K_{I1}$	67.33	$K_{I1}$	14.27
$K_{I2}$	80.60	$K_{I2}$	146.93
$K_{D1}$	0.80	$K_{D1}$	4.70
$K_{D2}$	3.50	$K_{D2}$	0.80
$\lambda$	0.20	$\lambda$	0.67
$\mu$	0.83	$\mu$	0.75

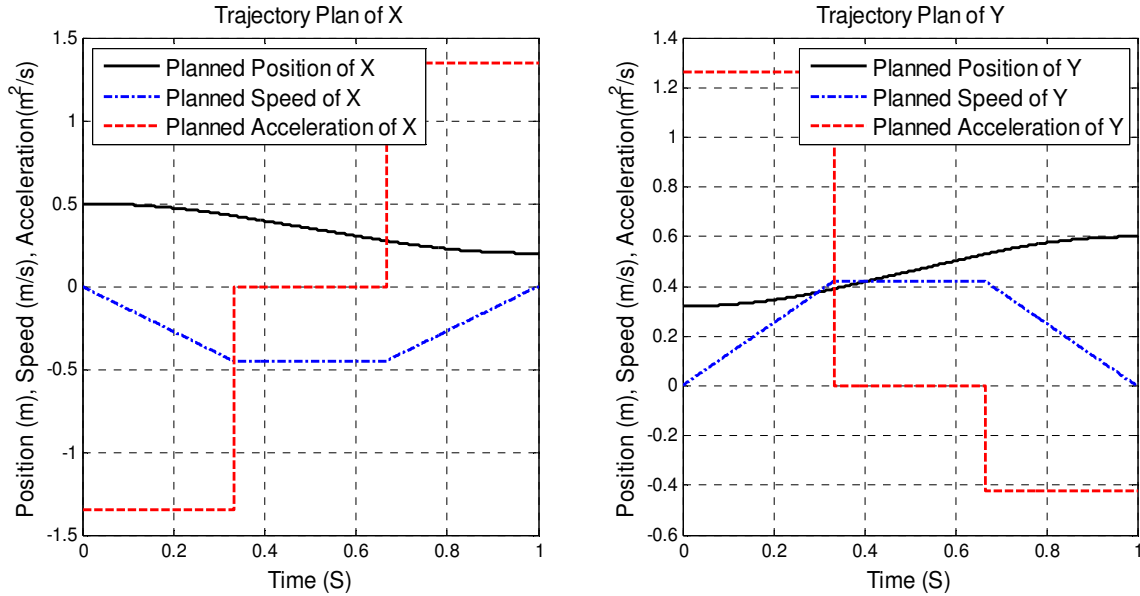


Figure 4. Trajectory Plan

## Simulation Results and Conclusions

Figure 5 shows a plot of the simulation results about the trajectory tracking. This figure includes the results from the system optimized by both the two-zone and three-zone methods. And, as a comparison, the authors included the results of an ordinary PID controller [15]. As shown in Figure 5, the optimized FoPID controllers have tracked the trajectory plan successfully. In terms of tracking error, the fractional system achieved a higher precision when compared with the ordinary PID system. Both the two-zone and three-zone methods provided satisfactory optimization results and, therefore, the optimization method studied here can be deemed effective. The tracking error at each sampling point was also recorded and the average squared tracking error computed, as summarized in Table 5. From Table 5, one can clearly see that the FoPID systems have raised the precision of tracking by one order of magnitude.

Table 5. Comparisons in terms of Mean Squared Tracking Errors

	Ordinary PID	FoPID, Two-Zones	FoPID, Three-Zones
Mean Squared Error in X	3.8859e-05	1.2279e-6	7.0355e-6
Mean Squared Error in Y	1.4879e-05	8.8149e-6	3.7683e-6

Evidenced by the simulation results, the FoPID controlled Adept550 robot system could achieve better results in terms of trajectory tracking. And the design methods introduced in this paper are effective for finding the optimized design of the fractional controllers. This method could be easily transferred into other applications related to fractional control and, consequently, bring valuable results to industrial practice.

In summary, then, the following conclusions are offered:

1. The fractional-order control of multilink robot systems always involves disturbance or other uncertainties; therefore, studying the limits of each eigenvalue is a feasible method for evaluating the overall stability. Furthermore, the boundary matrix could be helpful in finding the optimization design of the fractional-order controllers.
2. The stepwise penalized method could be used to optimize the design of FoPID systems, which allows people to move the system's eigenvalues toward to the desired regions. The method proposed in this paper could be generalized to other applications in the design of fractional-order controllers.
3. The optimized fractional system will take advantage of the enlarged stable region, while avoiding any negative effects brought by the increased number of eigenvalues. Simulation results show that the optimized FoPID controlled Adept550 system could track the planned trajectory successfully and raise the

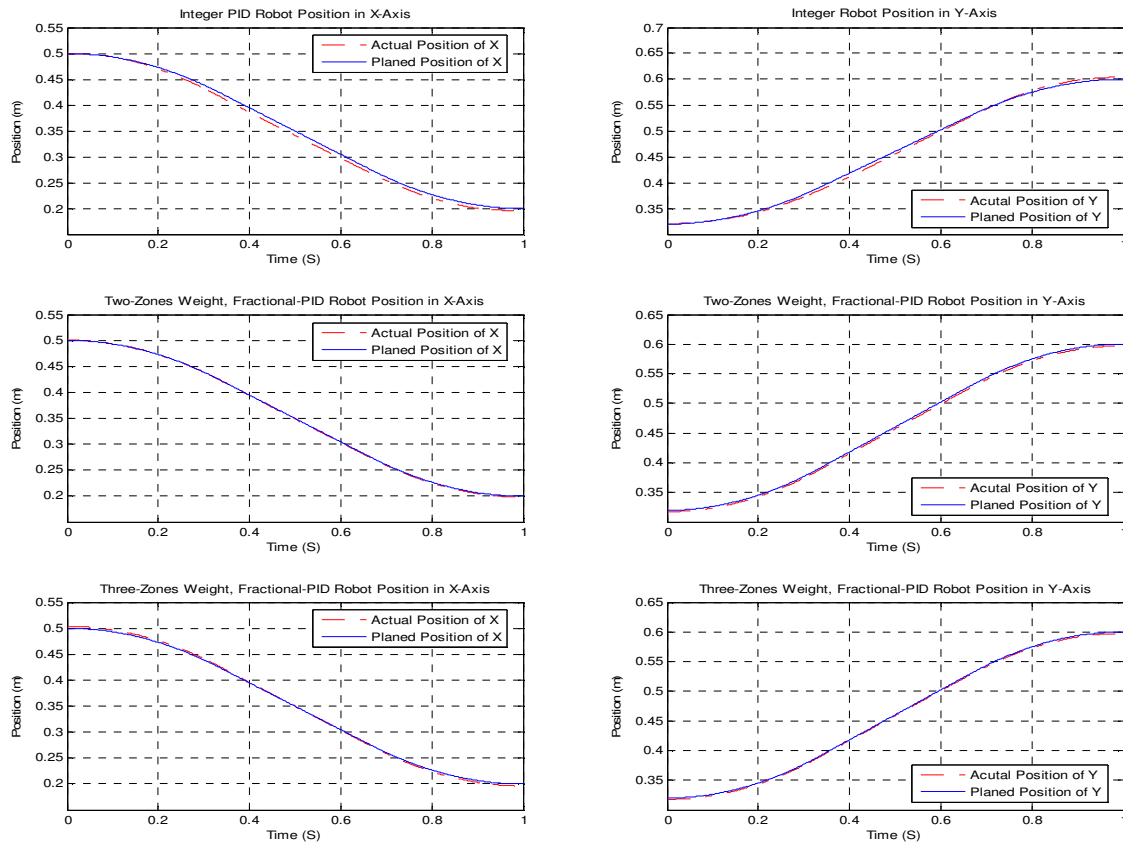


**Figure 5. Simulation Comparisons in terms of Trajectory**

precision greatly during the tracking process. This characteristic would bring valuable results to the manufacturing industry.

## References

- [1] Loverro, A. (2004). *Fractional Calculus: History, Definitions and Applications for the Engineer*. Unpublished report. Department of Aerospace and Mechanical Engineering. University of Notre Dame.
- [2] Mainardi, F. (1997). *Applications of Fractional Calculus in Mechanics, Transform Methods and Special Functions*. Varna'96, SCT Publishers, Singapore.
- [3] Rossikhin, Y. A. & Shitikova, M. V. (1997). Applications of Fractional Calculus to Dynamic Problems of Linear and Nonlinear Hereditary Mechanics of Solids. *Applied Mechanics Reviews*, 50, 15-67.
- [4] Bagley, R. L. & Calico, R. A. (1991). Fractional Order State Equations for the Control of Viscoelastically Damped Structures, *Journal of Guidance Control and Dynamics*, 14(2) 304-311.
- [5] Makroglou, A., Miller, R. K. & Skkar, S. (1994). Computational Results for a Feedback Control for a Rotating Viscoelastic Beam. *Journal of Guidance, Control and Dynamics*, 17(1), 84-90.
- [6] Oldham, K. B. (1976). A Signal Independent Electro-analytical Method. *Analytical Chemistry*, 72, 371-378.
- [7] Goto, M. & Ishii, D. (1975). Semi-differential Electro-analysis. *Electroanalytical Chemistry and Interfacial Electrochemistry*, 61, 361-365.
- [8] Matignon, D. (1998). *Generalized Fractional Differential and Difference Equations: Stability Properties and Modeling Issues*. Proc. Symposium for Math. Theory of Networks and Systems, Padova, Italy.
- [9] Diethelm, K., Ford, N. J., Freed, A. D. & Luchko, Y. (2005). Algorithms for the fractional calculus: A selection of numerical methods. *Computer Methods in Applied Mechanics and Engineering*. 194(6-8), 743-773.

- 
- [10] Podlubny, I. (1994). Fractional-Order Systems and Fractional-Order Controllers, Institute For Experimental Physics. *Slovak Academy of Sciences*, 4(2), 28-34.
- [11] Ying, L. & YangQuan, C. (2009). Fractional-order [proportional derivative] controller for robust motion control: Tuning procedure and validation. *American Control Conference*, (pp.1412-1417).
- [12] Dingyu, X. & YangQuan, C. (2006). Fractional Order Calculus and Its Applications in Mechatronic System Controls Organizers. *Proceedings of the 2006 IEEE International Conference on Mechatronics and Automation*, (pp. nil33-nil33).
- [13] Dingyu, X., Chunna, Z. & YangQuan, C. (2006). A Modified Approximation Method of Fractional Order System. *Proceedings of the 2006 IEEE International Conference on Mechatronics and Automation*, (pp. 1043-1048).
- [14] Sabatier, J., Moze, M. & Farges, C. (2010). LMI stability conditions for fractional order systems, Computers & Mathematics with Applications. *Fractional Differentiation and Its Applications*, 59(5), 1594-1609, ISSN 0898-1221.
- [15] Zhang, H. (2010). PID Controller Design for A Non-linear Motion Control Based on Modeling the Dynamics of Adept 550 Robot. *International Journal of Industrial Engineering and Management*, 1(1).
- [16] El-Sayed, A. M. A. (1994). Multivalued Fractional Differential Equations. *Applied Mathematics and Computation*, 80, 1-11.
- [17] Galkowski, K., Bachelier, O. & Kummert, A. (2006). Fractional Polynomials and nD Systems: A Continuous Case. *Decision and Control, 45th IEEE Conference*, (pp. 2913-2917).
- [18] Deif, A. S. (1991). The interval eigenvalue problem. *Applied Mathematics and Mechanics*, 71(1), 61-64.
- [19] YangQuan, C., Hyo-Sung, A. & Podlubny, I. (2005). Robust stability check of fractional order linear time invariant systems with interval uncertainties. *Mechatronics and Automation, 2005 IEEE International Conference*, 1(1), 210-215.
- [20] Qiu, Z., Müller, P. C. & Frommer, A. (2001). An approximation method for the standard interval eigenvalue problem of real nonsymmetric interval matrices. *Communications in Numerical Methods in Engineering*, 17, 239-251.

**H. HENRY ZHANG** is an assistant professor at Purdue University, his research covers control, applied fractional calculus, hydraulics, machining, and multi-discipline design optimization. Dr. Zhang got his PhD from the University of Michigan in June 1996. Dr. Zhang may be reached at [hhzhang@purdue.edu](mailto:hhzhang@purdue.edu)

**R. MARK FRENCH** is an associate professor at Purdue University. his research focuses on applied fractional calculus, music acoustics, aero elastics and optimization. Dr. French got his PhD from the University of Dayton. Dr. French may be reached at [rmfrench@purdue.edu](mailto:rmfrench@purdue.edu)

## Biographies

**YUEQUAN WAN** obtained PhD degree from Purdue University in May 2011. His research focuses on applied fractional calculus and fractional order control.